Turkish Journal of Electrical Engineering & Computer Sciences

http://journals.tubitak.gov.tr/elektrik/

Research Article

Turk J Elec Eng & Comp Sci
(2014) 22: 893 – 908

doi:10.3906/elk-1210-7

Multifunction converter based on Lyapunov function used in a photovoltaic system

Trung Nhan NGUYEN[1,2,*], **An LUO**[1]

[1]School of Electrical and Information Engineering, Hunan University, Hunan, P.R. China

[2]Faculty of Electrical Engineering, Industrial University of Ho Chi Minh City, Ho Chi Minh City, Vietnam

Received: 02.10.2012 • **Accepted:** 13.01.2013 • **Published Online:** 17.06.2014 • **Printed:** 16.07.2014

Abstract: The development of distributed generations (DGs) is essential to help solve energy crises and improve the reliability of electricity supplies. However, the involvement of a DG in a grid along with an increase of the nonlinear load will reduce the power quality. To solve this problem, we want the converter used in the DG to work flexibly, intelligently, and more accurately. To contribute to the improvement of quality of the DG, this paper proposes a multifunction converter (MFC) model. With the proposed model, the photovoltaic generator, which can be operated at harmonic suppression, and the power injection are more flexible than in the conventional controller used in DG. The controller of the MFC, which is designed based on the Lyapunov function, always ensures the stability of the system. Simulations and experimental results are presented to validate the correctness and effectiveness of the proposed model.

Key words: Active power filter, photovoltaic system, distributed generation, multifunction converter, stability theory

1. Introduction

In recent years, the issues of energy crises and environmental pollution have attracted the attention of countries all around the world. One direction of interest is looking for a clean energy (renewable energy) alternative to traditional fossil energy sources, where solar and wind energies are 2 correct and indispensable choices. The participation of renewable energy sources in the traditional power grid in the form of distributed generations (DGs) has formed a concept called a microgrid. In the 2 abovementioned renewable energies, solar energy seems more popularly exploited because of its advantages. Many research projects aiming at efficiently exploiting solar energy have been introduced. The model of the solar battery [photovoltaic (PV)] system was presented in [1–3]. Concerns about the method of determining the maximum power point tracking (MPPT) of the PV module were presented by Hussein et al. [4]. Issues related to the optimum configuration of PV modules have also received attention from researchers [5,6]. The PV system is an important module of a PV generator (PVG); it acts as a primary energy source for PVGs. For grid connection and power injection (POI) to the utility grid of PV systems, the DC-DC converter and the DC-AC inverter are used. The general model of a PVG connection and POI to the utility grid was presented in [7–9]. In such works, the full controlling method used in the PVG generates maximum output power and can be operated as the proposed reactive power compensator. With the controller presented in [7–9], the output reactive and active power of a PVG can be controlled at the same time, such as in a conventional synchronous generator in the power system.

*Correspondence: nguyentrungnhan@hui.edu.vn

As above, the development of the DG is essential to help solve energy crises and improve power supply reliability. However, the involvement of DGs on the main grid, along with the increase of the nonlinear load, leads to reduced power quality (mainly frequency oscillations, voltage fluctuations, and harmonic currents), in which the harmonic current is most interesting, especially in the grid-connected mode of the microgrid. One solution to reduce the harmonic currents in the grid generated by the DGs and nonlinear loads is to improve the control quality of the DC/AC inverters. In addition, the most effective technical solution is using active power filters (APFs). The model and control techniques of the APF were studied, implemented, and effectively applied in the utility grid [10], and then Luo et al. presented a new hybrid APF model, which can be applied in a medium- and high-voltage grid [11–14]. Energy sources to provide for the APF are usually taken from the main grid through a rectifier. Toward the use of solar energy in improving power quality, studies using PV systems as a primary energy supply for APFs were analyzed and presented in [15–17]. In addition, to exploit a solar radiation source efficiently, some flexible patterns combining the PV system and energy storage devices were studied and applied [18–20].

Everything presented above shows that the work on the exploitation and effective use of PV systems has been implemented and has satisfied our expectations. However, we expect the operating grid to be smarter, more flexible, reliable, and have better quality, especially in a microgrid system. For this, one of the basic requirements is that electrical devices in the utility grid work more adaptably and more intelligently. With such requirements, there are some further studies on this problem aiming to make the controller of the PVG more flexible, and they will be presented here. In [15,16], Wu et al. proposed a current controller based on amplitude-clamping and amplitude-scaling algorithms; the purposes of this control method are to prevent the output current from exceeding the switch rating and help a PVG change operation modes with more flexibility. Nevertheless, the determination of the inverter current command is too complicated in this proposed method. Moreover, in this work, active and reactive powers and distortions are controlled by complex control coefficients. The stability of the control system depends on the control coefficients and insecurity. Another solution for the grid-connected generation and harmonic compensation of the PV system is to adopt a dual-level inverter [21–23]. The advantages of this solution are a simple control and server and the dual purpose it gave the POI to utilize grid ability and, at the same time, solve the harmonic compensation problem. However, this is not an ideal solution, because it must be used through 2 insulated-gate bipolar transistor (IGBT) bridges (increasing the cost of implementation) and, actually, they work as 2 separate converters. To overcome such problems, a flexible control method through the harmonic voltage signals using a voltage source inverter (VSI) was introduced in [24,25]. With this control method, the reference signal for the control system of a PVG is the harmonic voltage, and a PVG can perform 2 functions simultaneously; it can inject power to the utility grid and reduce harmonic currents. However, the harmonic voltages are insignificant compared to the current, so the reference signal for the control system of the PVG based on the harmonic voltages will make the sensitivity of the system lower, especially in the grid-connected mode of the microgrid.

To contribute to the improvement of the quality and efficiency of the power electronic converters used in the PV system, this paper presents a flexible control model used in PVGs. With the proposed model, a PVG can automatically or manually switch control between the 2 modes [POI mode or harmonic suppression (HAS) mode], depending on the status of the utility grid, the weather conditions, and the requirements of the operator.

There are many control concepts and strategies for grid-connected converters, such as linear feedback control, nonlinear control, repetitive control, neural network approach, and adaptive control, that have been reported in the literature [26]. In this paper, the incorporated controller, based on the Lyapunov control

technique [26–28], allows flexible control of the operating modes and stability of PVG is proposed. Simulations and experimental results are provided to validate the correctness and effectiveness of the proposed model. The rest of paper organized as follows: configuration of the PVG is presented in Section 2 and the block diagrams of the control system of the PVG are presented in Section 3. Section 4 presents the multifunction controller (MFC) controller design method. Section 5 shows the simulation and experimental results in different cases. Finally, the conclusions are presented in Section 6.

2. System description

The configuration of the PVG is shown in Figure 1. It consists of a PV array connected to a series with a DC-DC converter, called a PV-DC source block. Next, the PV-DC source is connected to a series with the VSI, as shown in Figure 1 (note that in the dynamic analysis, the PV-DC source can be considered as an equivalent capacitor C_{pv}, as shown in Figure 1). In Figure 1, the inductor L_f and capacitor C_f form a low-pass L-C filter that removes the high-frequency switching harmonics generated by the VSI of the PVG. In fact, only the low-frequency harmonics (5th, 7th, and 11th) have a significant effect on the power quality of the main grid, so for simplicity in calculation, capacitor C_f can be omitted. The coupling inductor L_c (shown in Figure 1) acts as a connecting inductor, where its main role is to reduce the current oscillation when there is a closed-open connection between the PVG and the main grid. The amount of active power injected from the PVG is determined by the PV array output voltage and current. The MPPT control circuit is an important part of the

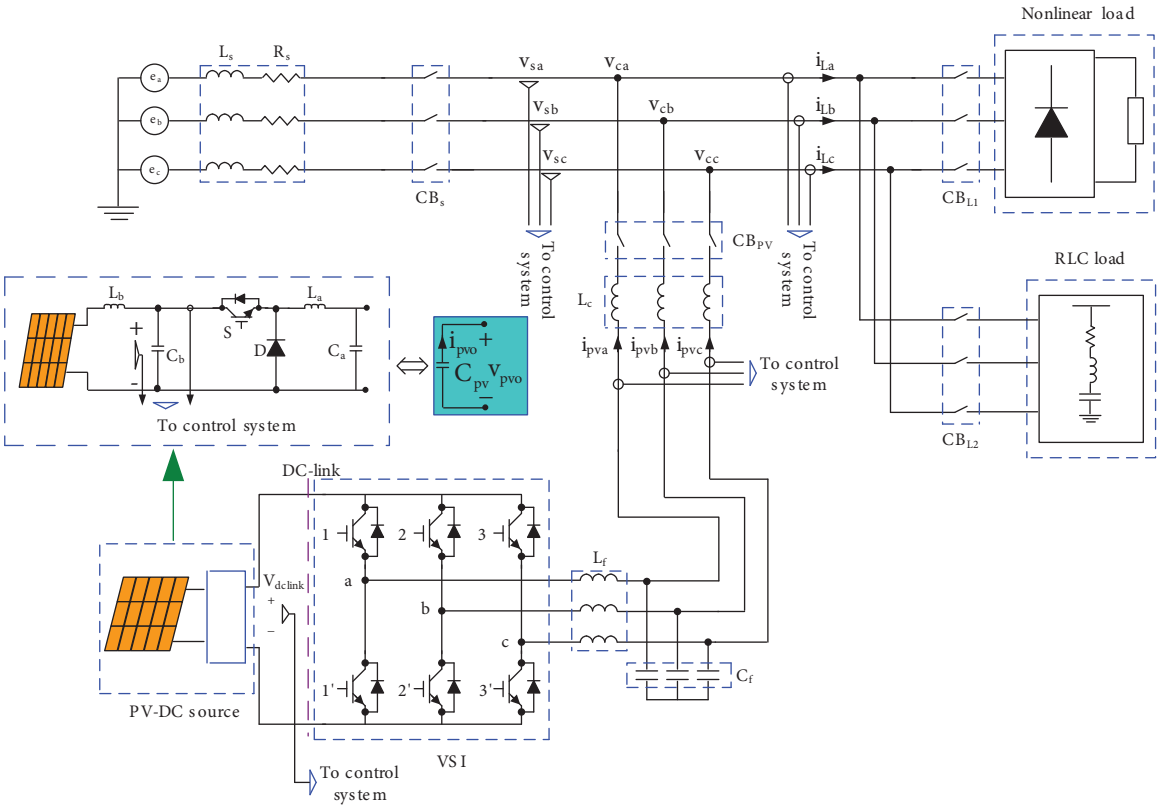

Figure 1. Configuration of the PVG.

PV-DC source; its objective is to set up the PV-array output reference voltage corresponding to the PV array maximum power [4]. The inputs of the MPPT controller are the output voltage and current of the PV array. The most important block in each PVG is the VSI, which acts not only as the DC-AC converter, but also as the MFC of the PVG in this work. The utility grid voltage at the command point and DC-link bus voltage are sensed through proper voltage-sensing circuitry; the actual load and PVG currents are sensed using a current sensor. The sensed signals become the input signals of the control system. The details of the multipurpose control method for the VSI based on the Lyapunov function are presented in the next section.

3. Block diagram of the control system

The block diagram control system of the PVG proposed in this paper is shown in Figure 2, which consists of a MPPT controller, phase-locked loop (PLL) module, 3-phase coordinates to the dq0 frame transformer, load harmonic current calculator, mode selector, determining control signal module based on the Lyapunov control technique, and pulse-width modulation generator. For the MPPT controller, to improve the efficiency of the PV system, we adopt a new topology for the DC-DC converter along with the global MPPT algorithm, which was proposed in [29] by Koutroulis et al.

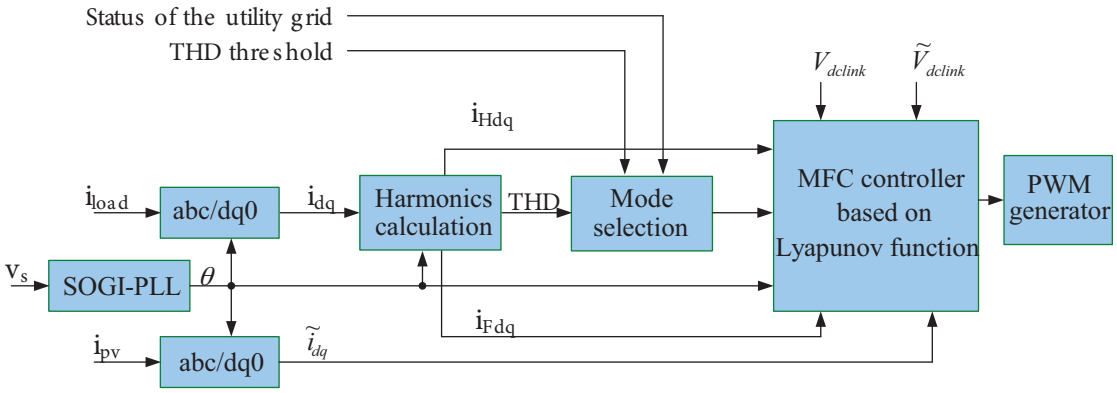

Figure 2. Block diagram of the control system used in the PVG.

In the proposed MPPT method, the maximum power points of the PV system are controlled by the PV-array side, whereas the harmonic currents of utility grid are controlled by the utility side. With the proposed system controller, the optimal output power of the PV system can be determined to achieve the desired features when the PVG is operated from injected power to the utility grid mode. With the PLL module, for simplicity of implementation and decrease of the time-delay, a PLL structure based on a second-order generalized integrator (SOGI-PLL) [30] is adopted in this work. The structure of the SOGI-PLL is shown in Figure 3.

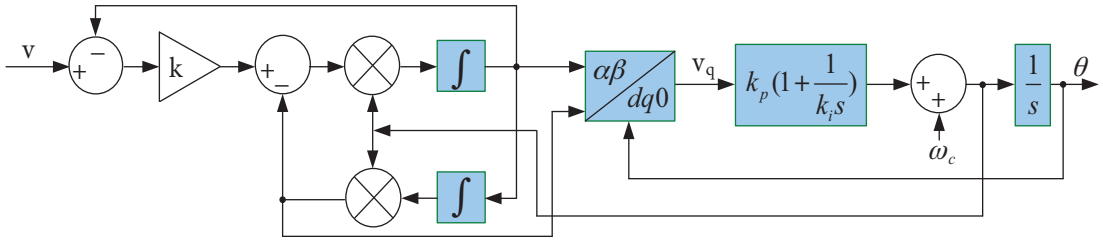

Figure 3. Diagram of the SOGI-PLL.

The correct estimation and measurement of harmonic currents are an important issue. If the power frequency of the signal is steady and near the nominal value, discrete Fourier transforms (DFTs) can be used and good estimation performance is achieved. However, there are considerable power frequency variations on an isolated system, such as a microgrid working in stand-alone mode. When these variations occur, they may introduce substantial phase errors in estimates using the DFT.

In order to deal with this problem and realize our aims in a digital signal processor (DSP) for real-time implementation easily, the sliding DFT (SDFT) [25,31] is used in load harmonic current calculation. The inside of the circuit diagram of the harmonic's calculation block, using the SDFT technique, is shown in Figure 4. The output of this block, respectively, is obtained using the fundamental current i_{Fdq}, the harmonic current i_{Hdq}, and the total harmonic distortion (THD) of the load current.

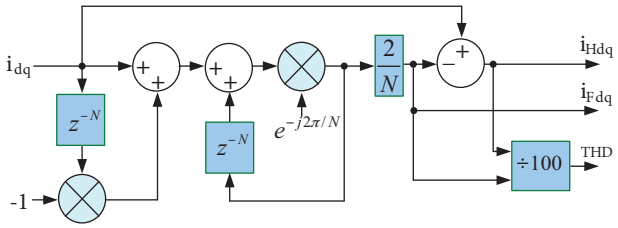

Figure 4. Diagram of the SDFT for fundamental, harmonic, and THD component calculations.

The next block is the mode selector; it allows the selection of operating situations. When selecting the manual mode, a PVG only operates in single-function mode (to inject power into the utility grid or suppress harmonic currents). In contrast to manual mode, in automatic mode, a MFC will automatically change the operating situation according to the input signals, such as the THD of the load current, the balance between the power generation and power demand status in the main grid, and weather conditions. The threshold of the input control signals can be changed through control programs.

The final block is the multifunction controller based on the Lyapunov control technique. This is the most important module; it is the center of the control system used in the PVG. The input signals of this block are the output signals of the mode selector, harmonic calculator, PLL block, and DC-link bus voltage. The main role of this block is to create a global switching function in the PWM generator module in both operating situations of the PVG (to inject power into the utility grid and suppress the harmonic currents). The details of this block are presented in the next section.

4. Multifunction controller design based on the Lyapunov function

4.1. Generalized mathematical model of the PVG

As mentioned above, for simplicity in the calculation, capacitor C_f can be ignored, and then an equivalent single-phase circuit of the PVG is shown in Figure 5, in which $R_{pv} \approx R_f + R_c$ and $L_{pv} \approx L_f + L_c$. Using Kirchoff's laws for circuits in Figure 5, we have:

$$-v_{c\xi o} - L_{pv}\dot{i}_{pv\xi} - R_{pv}i_{pv\xi} + v_{pv\xi} + v_{oo'} = 0, \tag{1}$$

$$C_{pv}\dot{V}_{dclink} - i_{dclink} = 0, \tag{2}$$

where $\xi = (a, b, c)$, $j = (a, b, c)$, and $v_{pv\xi} = v_{jo'}$ (note that the notation "$\bullet$" is the first-order differential per time). We are assuming that the electric load in all of the mode operations and the source supply voltages are

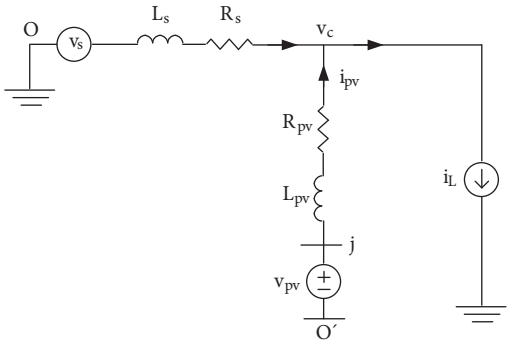

Figure 5. Equivalent single-phase circuit of the PVG.

balanced. Thus, $\sum_{\xi=(a,b,c)} v_{c\xi o} = \sum_{\xi=(a,b,c)} i_{pv\xi} = 0$ and from Eq. (1) we can deduce $v_{oo'} = -\frac{1}{3}\sum_{j=a}^{c} v_{jo'}$. Now we define switching function u_s of the IGBT bridge (see Figure 1) as follows:

$$u_s = \begin{cases} 1 \;\; if \;\; IGBT\ s\ ON\ and\ \ IGBT\ s'\ OFF \\ 0 \;\; if \;\; IGBT\ s\ OFF\ and\ \ IGBT\ s'\ ON \end{cases} ;\ s = \{1,2,3\}. \tag{3}$$

Thus, $v_{pv\xi} = u_s \mathrm{V}_{dclink}$. The differential Eq. (1) can be rewritten as follows:

$$-v_{c\xi o} - L_{pv}\dot{i}_{pv\xi} - R_{pv}i_{pv\xi} + (u_s - \frac{1}{3}\sum_{j=a}^{c} u_{jo'})V_{dclink} = 0. \tag{4}$$

Let us define a switching state function as follows:

$$\delta_{ns} = (u_s - \frac{1}{3}\sum_{j=a}^{c} u_{jo'}). \tag{5}$$

In fact, the 3-phase IGBT bridge only has 8 permissible switching states, so that Eq. (5) can be written as follows:

$$\delta_{ns} = \frac{1}{3} T_{ns} u_s^T, \tag{6}$$

where $T_{ns} = \begin{bmatrix} 2 & -1 & -1 \\ -1 & 2 & -1 \\ -1 & -1 & 2 \end{bmatrix}$ and $u_s = [u_1\ u_2\ u_3]$.

Please note that δ_{ns} has no zero-sequence component (i.e. $\Sigma\delta_{ns} = 0$), and in analysis of the PV-DC source of the system (see Figure 1), we have:

$$\dot{V}_{dclink} = \frac{i_{dclink}}{C_{pv}} = \frac{1}{C_{pv}}\sum_{\xi=a}^{c} u_\xi i_{pv\xi} \tag{7}$$

and

$$\sum_{s=1}^{3} \delta_{ns} = \sum_{j=a}^{c} u_j i_{pvj}. \tag{8}$$

Substituting in Eq. (2), we have (note that $i_{pv1} = i_{pva}$, and $i_{pv2} = i_{pvb}$):

$$\dot{V}_{dclink} = \frac{1}{C_{pv}} \sum_{k=1}^{2} [(3-k)\delta_{n1} + k\delta_{n2}] i_{pvk}. \tag{9}$$

Any vector on the abc stationary reference frame can be expressed on the dq0 synchronous reference frame using the Park transformation [32]. Thus, the transformation matrix to translate a current vector from the abc stationary reference frame to the dq0 synchronous reference frame is given by:

$$i_{dq0} = T_\theta i_{abc}, \tag{10}$$

where

$$T_\theta = \sqrt{\frac{2}{3}} \begin{bmatrix} \cos(\theta) & \cos(\theta - \frac{2\pi}{3}) & \cos(\theta + \frac{2\pi}{3}) \\ -\sin(\theta) & -\sin(\theta - \frac{2\pi}{3}) & -\sin(\theta + \frac{2\pi}{3}) \\ \frac{1}{\sqrt{2}} & \frac{1}{\sqrt{2}} & \frac{1}{\sqrt{2}} \end{bmatrix}.$$

The resulting transformed model in the dq0 synchronous reference frame is given by:

$$\begin{aligned} &-v_{cd} - L_{pv}\dot{i}_{pvd} - R_{pv} i_{pvd} + \omega L_{pv} i_{pvq} + \delta_{nd} V_{dclink} = 0 \\ &-v_{cq} - L_{pv}\dot{i}_{pvq} - R_{pv} i_{pvq} - \omega L_{pv} i_{pvd} + \delta_{nq} V_{dclink} = 0 \\ &C_{pv}\dot{V}_{dclink} = \delta_{nd} i_{pvd} + \delta_{nq} i_{pvq} \end{aligned} . \tag{11}$$

Eq. (11) can be rearranged in the following form:

$$\begin{aligned} \dot{i}_{pvd} &= -\tfrac{R_{pv}}{L_{pv}} i_{pvd} + \omega i_{pvq} + \tfrac{1}{L_{pv}} \delta_{nd} V_{dclink} - \tfrac{v_{cd}}{L_{pv}} \\ \dot{i}_{pvq} &= -\tfrac{R_{pv}}{L_{pv}} i_{pvq} - \omega i_{pvd} + \tfrac{1}{L_{pv}} \delta_{nq} V_{dclink} - \tfrac{v_{cq}}{L_{pv}} \\ \dot{V}_{dclink} &= \tfrac{1}{C_{pv}} (\delta_{nd} i_{pvd} + \delta_{nq} i_{pvq}) \end{aligned} . \tag{12}$$

Let us choose $x_1 = i_{pvd} - \tilde{i}_{pvd}$, $x_2 = i_{pvq} - \tilde{i}_{pvq}$, and $x_3 = \mathrm{V}_{dclink} - \tilde{V}_{dclink}$, where x_1, x_2, and x_3 are the state variables of the MFC system and $\tilde{i}_{pvd}$, $\tilde{i}_{pvq}$, and $\tilde{V}_{dclink}$ are the reference currents calculated from the load and the reference voltage at DC-link bus. Substituting these values into Eq. (12), we have:

$$\begin{aligned} \dot{x}_1 &= -\tfrac{R_{pv}}{L_{pv}} x_1 + \omega x_2 + \delta_{nd} \tfrac{x_3 + \tilde{V}_{dclink}}{L_{pv}} - \tfrac{\Delta_{nd}}{L_{pv}} \tilde{V}_{dclink} \\ \dot{x}_2 &= -\tfrac{R_{pv}}{L_{pv}} x_2 - \omega x_1 + \delta_{nq} \tfrac{x_3 + \tilde{V}_{dclink}}{L_{pv}} - \tfrac{\Delta_{nq}}{L_{pv}} \tilde{V}_{dclink} \\ \dot{x}_3 &= \tfrac{1}{C_{pv}} [\delta_{nd}(x_1 + \tilde{i}_{pvd}) + \delta_{nq}(x_2 + \tilde{i}_{pvq}) - \Delta_{nd}\dot{\tilde{i}}_{pvd} - \Delta_{nd}\dot{\tilde{i}}_{pvq}] \end{aligned} , \tag{13}$$

where Δ_{nd}, Δ_{nq} are the steady-state switching functions and δ_{nd}, δ_{nq} are the global switching functions [26]. The steady-state switching functions are given by:

$$\begin{aligned} \Delta_{nd} &= \tfrac{L_{pv}}{\tilde{V}_{dclink}} (-\dot{\tilde{i}}_d - \tfrac{R_{pv}}{L_{pv}} \tilde{i}_d + \omega \tilde{i}_q + \tfrac{v_{cd}}{L_{pv}}) \\ \Delta_{nq} &= \tfrac{L_{pv}}{\tilde{V}_{dclink}} (-\dot{\tilde{i}}_q - \tfrac{R_{pv}}{L_{pv}} \tilde{i}_q - \omega \tilde{i}_d + \tfrac{v_{cq}}{L_{pv}}) \end{aligned} . \tag{14}$$

4.2. Control strategy based on the Lyapunov function

According to Lyapunov's stability theorem [27], a nonlinear system is a globally asymptotical stability if the Lyapunov candidate V(x) function satisfies the following properties (notation $\forall x$ means that it is for all x).

$$\begin{cases} V(0) = 0 \\ V(x) > 0, & \forall x \neq 0 \\ \dot{V}(x) < 0, & \forall x \neq 0 \\ V(x) \to \infty, & \forall x \to \infty \end{cases} \tag{15}$$

In this paper, the Lyapunov function is defined as the storage energy of the MFC and it is given as:

$$V = L_{pv}x_1^2 + L_{pv}x_2^2 + C_{pv}x_3^2. \tag{16}$$

Now substituting into Eqs. (13) and (15), we have the following.

$$\begin{aligned} \dot{V}(x) &= \frac{\partial V}{\partial x}.\frac{\partial x}{\partial t} = \frac{\partial V}{\partial x_1}\dot{x}_1 + \frac{\partial V}{\partial x_2}\dot{x}_2 + \frac{\partial V}{\partial x_3}\dot{x}_3 = -2R_{pv}x_1^2 - 2R_{pv}x_2^2 + \\ &+\delta_{nd}[2x_3\tilde{i}_{pvd} + 2x_1(\tilde{V}_{dclink} + x_3)] + \delta_{nq}[2x_3\tilde{i}_{pvq} + 2x_2(\tilde{V}_{dclink} + x_3)] - \\ &-\Delta_{nd}(2x_3\tilde{i}_{pvd} + 2x_1\tilde{V}_{dclink}) - \Delta_{nq}(2x_3\tilde{i}_{pvq} + 2x_2\tilde{V}_{dclink}) \end{aligned} \tag{17}$$

Note that $\tilde{V}_{dclink} \gg x_3$ and so can be approximated as $\tilde{V}_{dclink} + x_3 \approx \tilde{V}_{dclink}$, and then Eq. (17) can be rewritten as follows:

$$\begin{aligned} \dot{V}(x) &= -2R_{pv}x_1^2 - 2R_{pv}x_2^2 - (2x_3\tilde{i}_{pvd} + 2x_1\tilde{V}_{dclink})(\Delta_{nd} - \delta_{nd}) \\ &-(2x_3\tilde{i}_{pvq} + 2x_2\tilde{V}_{dclink})(\Delta_{nq} - \delta_{nq}) \end{aligned}. \tag{18}$$

Eq. (18) shows that the Lyapunov function derivative always becomes negatively definite if the switching state functions are chosen as follows:

$$\begin{cases} \delta_{nd} = \Delta_{nd} - G(2x_3\tilde{i}_{pvd} + 2x_1\tilde{V}_{dclink}) \\ \delta_{nq} = \Delta_{nq} - G(2x_3\tilde{i}_{pvq} + 2x_2\tilde{V}_{dclink}) \end{cases} \qquad G > 0, \tag{19}$$

where G is the gain of the controller used in the MFC.

In order to ensure the global stability of the proposed control system, we establish the state equations of the MFC system at around the equilibrium point and assess its stability through the root locus method. The state equations of the MFC system can be obtained by substituting Eq. (19) into Eq. (13), where we have:

$$\begin{bmatrix} \dot{x}_1 \\ \dot{x}_2 \\ \dot{x}_3 \end{bmatrix} = \begin{bmatrix} -\frac{R_{pv}+2G\tilde{V}_{dclink}^2}{L_{pv}} & \omega & -\frac{2G\tilde{i}_d\tilde{V}_{dclink}}{L_{pv}} \\ -\omega & -\frac{R_{pv}+2G\tilde{V}_{dclink}^2}{L_{pv}} & -\frac{2G\tilde{i}_q\tilde{V}_{dclink}}{L_{pv}} \\ \frac{\Delta_{nd}-2G\tilde{V}_{dclink}\tilde{i}_d}{C_{pv}} & \frac{\Delta_{nq}-2G\tilde{V}_{dclink}\tilde{i}_q}{C_{pv}} & -\frac{2G(\tilde{i}_d^2+\tilde{i}_q^2)}{C_{pv}} \end{bmatrix} . \begin{bmatrix} x_1 \\ x_2 \\ x_3 \end{bmatrix}. \tag{20}$$

From Eq. (20), the characteristic equation of the closed-loop control system is given as:

$$s^3 + as^2 + bs + c = 0, \tag{21}$$

where

$$a = \frac{G[C_{pv}\tilde{V}_{dclink}^2 + L_{pv}(\tilde{i}_d^2 + \tilde{i}_q^2) + 2R_{pv}C_{pv}]}{L_{pv}C_{pv}}, \quad b \approx \frac{(\omega L_{pv})^2 + GL_{pv}\tilde{V}_{dclink}^2 + GR_{pv}\tilde{V}_{dclink}^2}{L_{pv}^2},$$

and

$$c \approx \frac{(G^2R_{pv}\tilde{V}_{dclink}^2 + GL_{pv}\omega\tilde{V}_{dclink}^2)(\tilde{i}_d^2+\tilde{i}_q^2) - G^2L_{pv}\omega\tilde{V}_{dclink}^2(\tilde{i}_d\tilde{i}_q+\tilde{i}_q^2) + G^2R_{pv}\tilde{i}_d^2\tilde{V}_{dclink}^2}{L_{pv}^2C_{pv}} + \frac{G^2R_{pv}\tilde{V}_{dclink}^2\tilde{i}_d\tilde{i}_q - \Delta_{nd}\Delta_{nq}G\tilde{V}_{dclink}^2 + \Delta_{nq}GR_{pv}\tilde{i}_d\tilde{V}_{dclink}^3}{L_{pv}^2C_{pv}}.$$

If the resistance is ignored ($R_{pv} = 0$) and there is only the active POI to the utility grid in POI mode ($i_q = 0$), the coefficients of Eq. (21) are defined simply as:

$$a = \frac{GC_{pv}\tilde{V}_{dclink}^2 + L_{pv}\tilde{i}_d^2}{L_{pv}C_{pv}}, \quad b \approx \frac{(\omega L_{pv})^2 + GL_{pv}\tilde{V}_{dclink}^2}{L_{pv}^2}, \quad c \approx \frac{GL_{pv}\omega\tilde{V}_{dclink}^2\tilde{i}_d^2 - \Delta_{nd}\Delta_{nq}G\tilde{V}_{dclink}^2}{L_{pv}^2C_{pv}}.$$

The root locus of the characteristic in Eq. (21) is shown in Figure 6, where it is clear that all of the poles are in the left-half plane; therefore, one deduces that the system is globally stable. Please note that the choice of the gain of controller G is based on the fast response of the closed-loop system and the good quality of the HAS mode and power injection in the POI mode. In fact, the control system is sufficiently fast when the value of G is sufficiently large. However, this value relates to the efficiency operation of the MFC system, such that the value of G is often chosen as less than 1. In this work, the value of G is chosen as equal to 0.1.

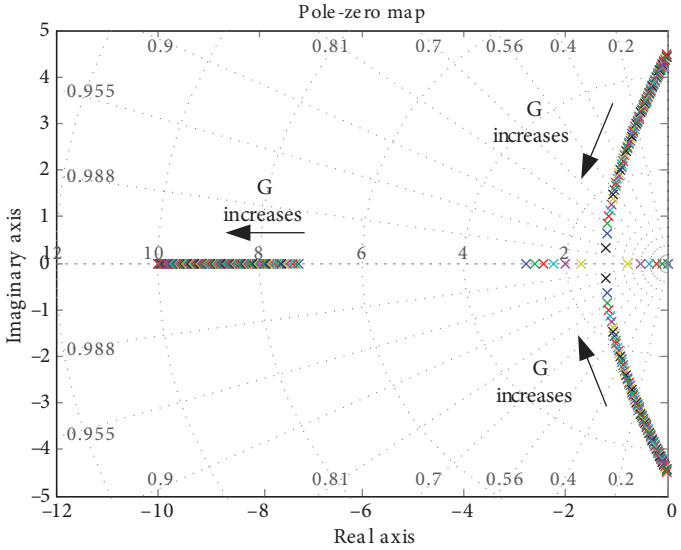

Figure 6. Root locus with the variable gain of the controller (arrow direction).

5. Simulation and experimental results

5.1. Simulation results

The proposed MFC, along with flexible control strategies based on Lyapunov's stability theory, are verified through simulation in the MATLAB/Simulink environment. The main purpose of the simulation is to test the flexibility of the control strategies used in a PVG in different modes. The specification parameters used in these simulations are given in the Table below.

Table. Specification parameters in the simulation.

AC grid line-line voltage	V_s = 380 V (rms)
AC grid frequency	f = 50 Hz
Source impedance	L_s = 0.2 mH, R_s = 0.08 Ω
Low-pass L-C filter	R_f = 0.1 Ω, L_f = 1 mH, C_f = 0.1 μF
Coupling inductor	R_c = 0.1 Ω, L_c = 1 mH
k_p (using in SOGI-PLL)	2.5
k_i (using in SOGI-PLL)	0.02
Switching frequency	f_s = 10,000 Hz

First, we consider a fixed nonlinear load case (CB_{L1} is closed). Figure 7 illustrates the simulation results of the PVG in this case, where at 0.1 s, the control system is changed from POI mode to harmonic suppression mode (from POI mode to HAS mode).

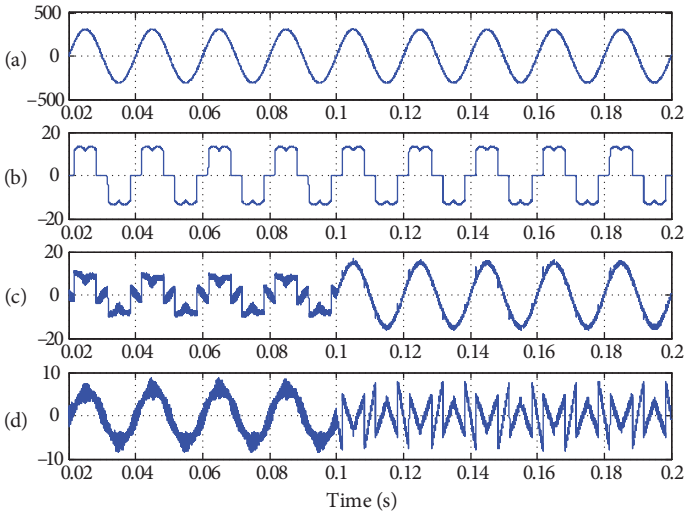

Figure 7. Waveform diagrams of the a-phase voltage and current in the fixed nonlinear load case: a) the grid voltage, b) the load current, c) the grid current, and d) the PVG current.

It can be seen from Figure 7 that the responses generated by applying the proposed MFC along with the Lyapunov control technique have brought us what we expected (satisfies the current and voltage harmonic limits as specified by IEEE-519-1992) [33].

The power responses generated by applying the proposed PVG system (in phase a) are shown in Figure 8. It is obvious that the load power is supplied by the maximum power extracted from the PV system and the main grid when the PVG is operated in POI mode (before t = 0.1 s). Alternately, when the PVG is operated in HAS mode (after t = 0.1 s), the load harmonic currents are eliminated (the corresponding THD of the supply current is reduced from 30.45% before t = 0.1 s to 4.92% after t = 0.1 s), while the power extracted from the PV system is almost 0 (see Figure 8). In addition, the harmonic voltage has changed very little over the operating modes (the THD changed from 0.81% to 1.61%).

We now consider a variable load from the linear load (the THD of the load current is less than the threshold THD) to the nonlinear load (the THD of load current exceeds the threshold THD) case. The change occurs at t = 0.1 s and happens through 2 circuit breakers, CB_{L1} and CB_{L2}. At that time, the PVG system will automatically change from POI mode to HAS mode.

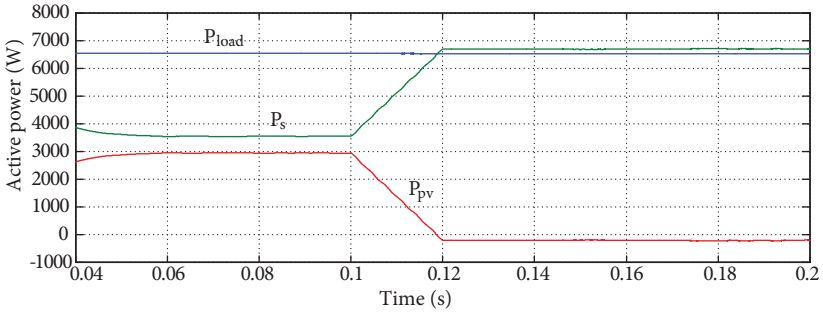

Figure 8. The power responses of the proposed PVG system in the fixed nonlinear load case.

Figure 9 demonstrates the responses of the MFC current and voltage over time in this case. The responses to the load power, main grid power, and power extracted from the PV system are shown in Figure 10.

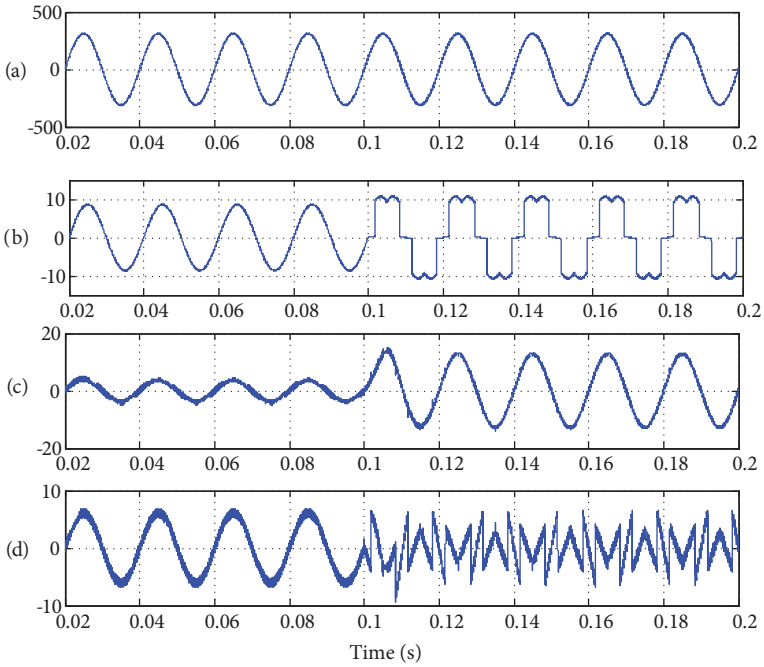

Figure 9. Waveform diagrams of the a-phase voltage and current in variable load cases: a) the grid voltage, b) the load current, c) the grid current, and d) the PVG current.

These figures show that the controller of the proposed MFC operates correctly in both POI mode and HAS mode. Moreover, similar to the fixed nonlinear load case above, the proposed MFC system always reaches the maximum power extracted from the PV system in POI mode and eliminates harmonic currents efficaciously (satisfies standard IEEE-519-1992) in HAS mode (see Figure 11), as we expect from its functions. The flexibility and rapidly dynamic response ability are also the advantages of the proposed MFC.

5.2. Experimental results

To confirm the effectiveness of the PVG with the proposed topology and control strategy, some experiments are done employing a laboratory test system on a 60-kVA setup. A TI TMS320F2812 DSP is used to implement the control methods based on Eqs. (14) and (18). The control parameters are the same as those in the simulations

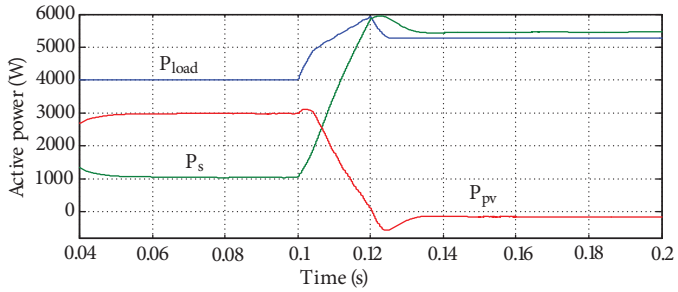

Figure 10. The power responses of the proposed PVG system in the variable load case.

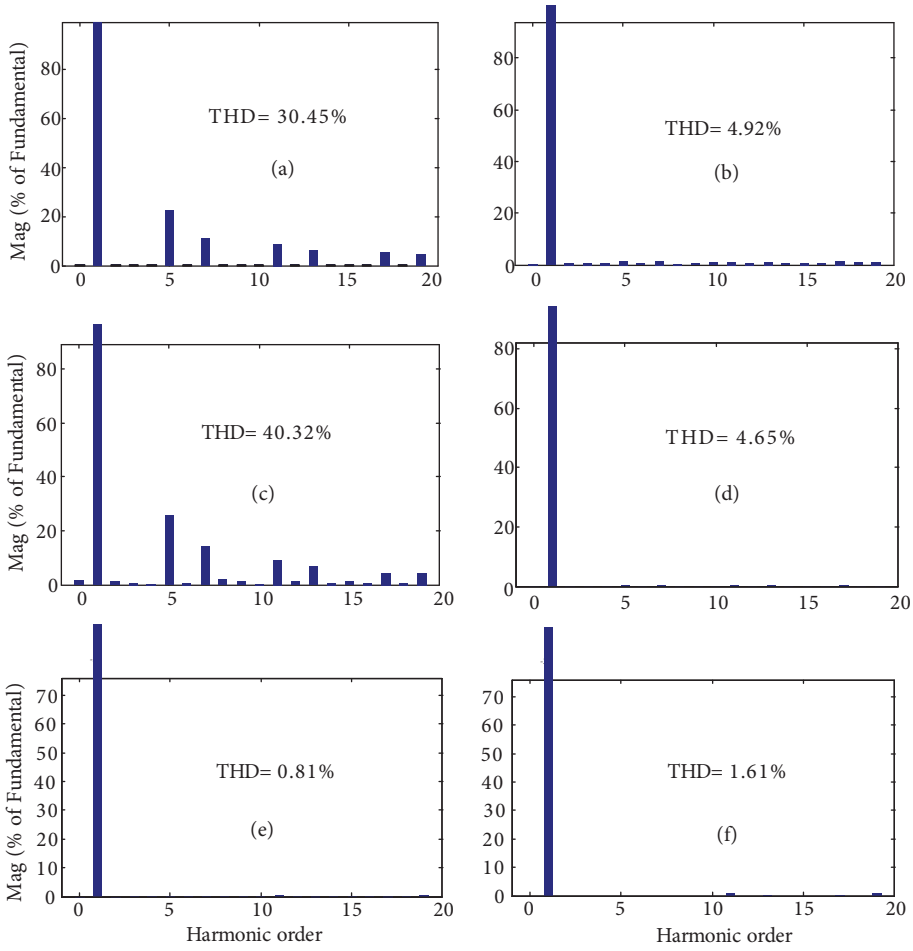

Figure 11. Spectrum diagrams of the currents and voltages in Figures 7 and 9: a) THD of the grid current when the MFC is operated in POI mode in the fixed nonlinear load case, b) THD of the grid current when the MFC is operated in HAS mode in the fixed nonlinear load case, c) THD of the load current is changed from linear (0.81%) to nonlinear (40.32%), d) THD of the grid current after the MFC automatically changes the operation mode, e) THD of the grid voltage without a PVG system, and f) THD of the grid voltage with a PVG system.

(as shown in the Table) and can be changed through the keyboard. The PV arrays, voltage-source IGBT inverter, and DSP-based controller are shown in Figure 12. The experimental results for the operation modes are shown in Figure 13.

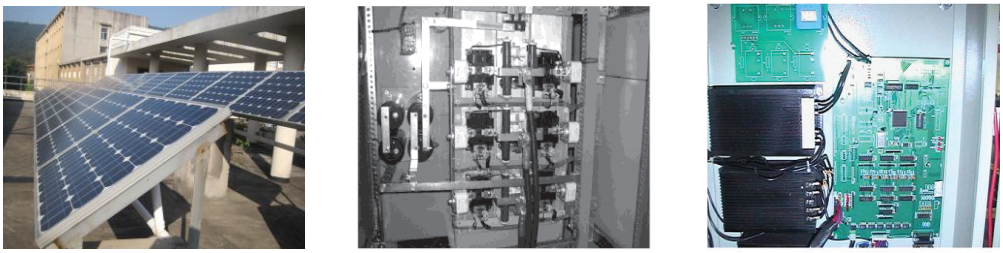

(a) (b) (c)

Figure 12. The experimental equipment of the PVG: a) PV array, b) voltage-source IGBT inverter, and c) DSP-based controller.

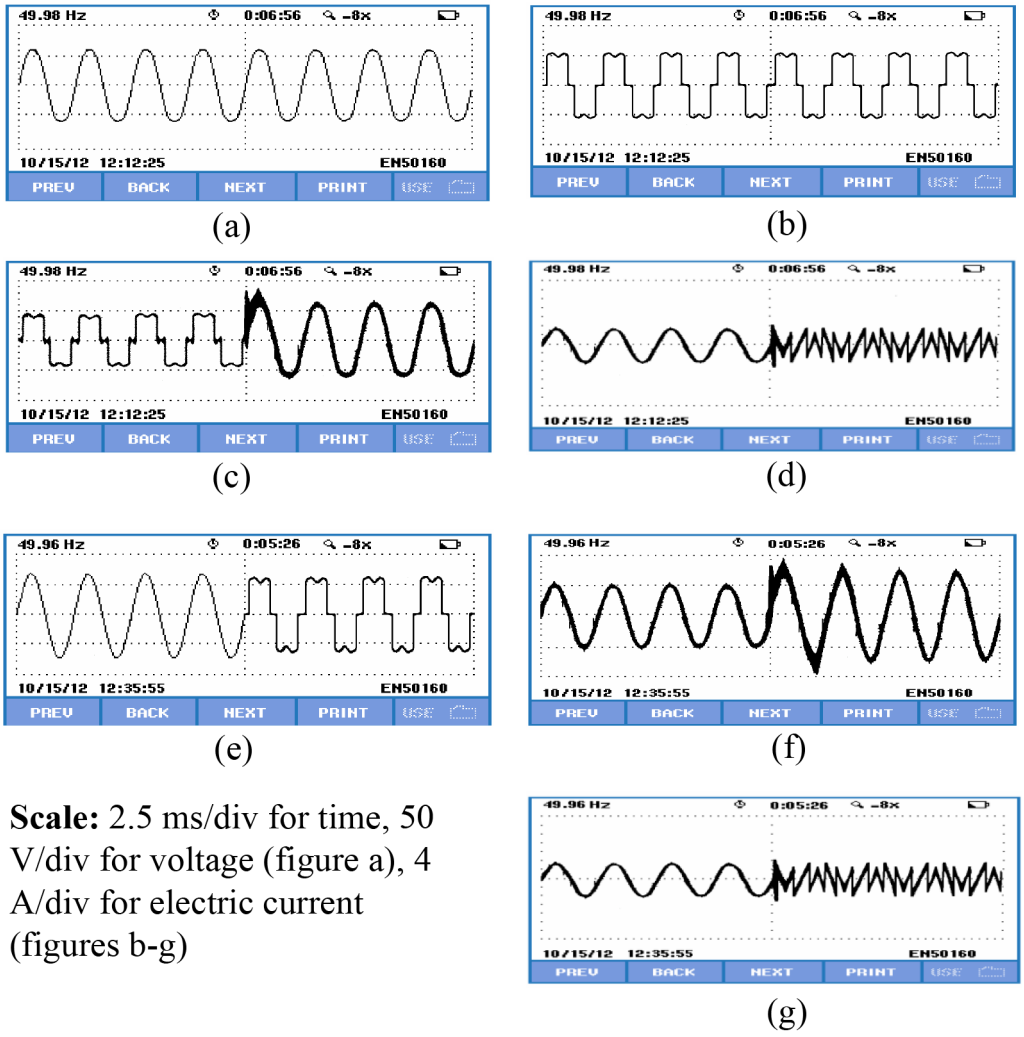

Figure 13. Experimental results (all values in phase a): a) grid voltage, b) load current in the fixed nonlinear load case, c) grid current in the fixed nonlinear load case, d) PVG current in the fixed nonlinear load case, e) load current in variant load cases, f) grid current in variant load cases, and g) PVG current in variant load cases.

From Figure 13, it can be seen that the Lyapunov function-based controller of the proposed PVG is operated correctly in both POI mode and HAS mode. It is also shown that the proposed controller has good steady-state and dynamic response characteristics whether the load is changed or not.

6. Conclusion

This paper proposes a MFC with a Lyapunov function-based controller that allows the flexible control of the operating modes and always ensures the stability of the system. The MFC configuration and control principles were analyzed in detail. It was shown that the proposed Lyapunov function-based incorporated controller can operate at harmonic suppression and POI, which is more flexible than a conventional controller used in DG. In addition, the SOGI-PLL and SDFT techniques were used in this paper to contribute to the decrease in the phase errors, the time delay, and harmonic current extraction exactly. This makes the MFC operation more accurate and its dynamic responses faster. The simulation and experimental results were presented to validate the correctness and effectiveness of the proposed model.

It should be noted that using the same PVG structure for both the purpose of reducing the harmonic currents and POI will be very difficult to implement if using conventional control methods. However, in this paper, the control method is based on the energy function of the results achieved as we expected, and the global stability of the system was also validated through Eq. (21) and Figure 6. This is a new contribution of this paper.

References

[1] M.G. Villalva, J.R. Gazoli, E.R. Filho, "Modeling and circuit-based simulation of photovoltaic arrays", Brazilian Power Electronics Conference, pp. 1244–1254, 2009.

[2] A.H.M. Nordin, A.M. Omar, "Modeling and simulation of photovoltaic (PV) array and maximum power point tracker (MPPT) for grid-connected PV system", 3rd International Symposium and Exhibition in Sustainable Energy and Environment, pp. 114–119, 2011.

[3] Y. Mahmoud, W. Xiao, H.H. Zeineldin, "A simple approach to modeling and simulation of photovoltaic modules", IEEE Transactions on Sustainable Energy, Vol. 3, pp. 185–186, 2012.

[4] K.H. Hussein, I. Muta, T. Hoshino, M. Osakada, "Maximum photovoltaic power tracking: an algorithm for rapidly changing atmospheric conditions", IEE Proceedings - Generation, Transmission, and Distribution, Vol. 142, pp. 59–64, 1995.

[5] G.V. Quesada, F.G. Gispert, R.P. Lopez, M.R. Lumbreras, A.C. Roca, "Electrical PV array reconfiguration strategy for energy extraction improvement in grid-connected PV systems", IEEE Transactions on Industrial Electronics, Vol. 56, pp. 4319–4331, 2009.

[6] L.F.L. Villa, D. Picault, B. Raison, S. Bacha, A. Labonne, "Maximizing the power output of partially shaded photovoltaic plants through optimization of the interconnections among its modules", IEEE Journal of Photovoltaics, Vol. 2, pp. 154–163, 2012.

[7] L.B. Wu, Z.M. Zhao, J.Z. Liu, "A single-stage three-phase grid-connected photovoltaic system with modified MPPT method and reactive power compensation", IEEE Transactions on Energy Conversion, Vol. 22, pp. 881–886, 2007.

[8] M.G. Molina, P.E. Mercado, "Modeling and control of grid-connected photovoltaic energy conversion system used as a dispersed generator", Transmission and Distribution Conference and Exposition: Latin America, pp. 1–8, 2008.

[9] F. Delfino, G.B. Denegri, M. Invernizzi, R. Procopio, "An integrated active and reactive power control scheme for grid-connected photovoltaic production systems", IEEE Conference on Power Electronics Specialists, pp. 1463–1468, 2008.

[10] B. Singh, K. Al-Haddad, A. Chandra, "A review of active filters for power quality improvement", IEEE Transactions on Industrial Electronics, Vol. 46, pp. 960–971, 1999.

[11] A. Luo, C. Tang, Z.K. Shuai, W. Zhao, F. Rong, K. Zhou, "A novel three-phase hybrid active power filter with a series resonance circuit tuned at the fundamental frequency", IEEE Transactions on Industrial Electronics, Vol. 56, pp. 2431–2440, 2009.

[12] A. Luo, Z.K. Shuai, W.J. Zhu, R.X. Fan, C.M. Tu, "Development of hybrid active power filter based on the adaptive fuzzy dividing frequency-control method", IEEE Transactions on Power Delivery, Vol. 24, pp. 424–432, 2009.

[13] Z.K. Shuai, A. Luo, W.J. Zhu, R.X. Fan, K. Zhou, "Study on a novel hybrid active power filter applied to a high-voltage grid", IEEE Transactions on Power Delivery, Vol. 24, pp. 2344–2352, 2009.

[14] A. Luo, S.J. Peng, C.P. Wu, J.B. Wu, Z.K. Shuai, "Power electronic hybrid system for load balancing compensation and frequency-selective harmonic suppression", IEEE Transactions on Industrial Electronics, Vol. 59, pp. 723–732, 2012.

[15] T.F. Wu, H.S. Nien, C.L. Shen, T.M. Chen, "A single-phase inverter system for PV power injection and active power filtering with nonlinear inductor consideration", IEEE Transactions on Industry Applications, Vol. 41, pp. 1075–1083, 2005.

[16] T.F. Wu, H.S. Nien, H.M. Hsieh, C.L. Shen, "PV power injection and active power filtering with amplitude-clamping and amplitude-scaling algorithms", IEEE Transactions on Industry Applications, Vol. 43, pp. 731–741, 2007.

[17] M. Cirrincione, M. Pucci, G. Vitale, "A single-phase DG generation unit with shunt active power filter capability by adaptive neural filtering", IEEE Transactions on Industrial Electronics, Vol. 55, pp. 2093–2110, 2008.

[18] S.J. Chiang, H.J. Shieh, M.C. Chen, "Modeling and control of PV charger system with SEPIC converter", IEEE Transactions on Industrial Electronics, Vol. 56, pp. 4344–4353, 2009.

[19] H.J. Chiu, Y.K. Lo, C.J. Yao, T.P. Lee, J.M. Wang, J.X Lee, "A modular self-controlled photovoltaic charger with interintegrated circuit (I^2C) interface", IEEE Transactions on Energy Conversion, Vol. 26, pp. 281–289, 2011.

[20] H. Fakham, D. Lu, B. Francois, "Power control design of a battery charger in a hybrid active PV generator for load-following applications", IEEE Transactions on Industrial Electronics, Vol. 58, pp. 85–94, 2011.

[21] Y.W. Li, D.M. Vilathgamuwa, P.C. Loh, "Microgrid power quality enhancement using a three-phase four-wire grid-interfacing compensator", IEEE Transactions on Industry Applications, Vol. 41, pp. 1707–1719, 2005.

[22] J. Li, F. Zhuo, X.W. Wang, L. Wang, S. Ni, "A grid-connected PV system with power quality improvement based on boost + dual-level four-leg inverter", IEEE Conference on Power Electronics and Motion Control, pp. 436–440, 2009.

[23] J. Li, F. Zhuo, J.J. Liu, X.W. Wang, B. Wen, L. Wang, S. Ni, "Study on unified control of grid-connected generation and harmonic compensation in dual-stage high-capacity PV system", IEEE Conference on Energy Conversion Congress and Exposition, pp. 3336–3342, 2009.

[24] C.J. Gajanayake, D. M. Vilathgamuwa, P.C. Loh, R. Teodorescu, F. Blaabjerg, "Z-Source inverter-based flexible distributed generation system solution for grid power quality improvement", IEEE Transactions on Energy Conversion, Vol. 24, pp. 695–704, 2009.

[25] J.W. He, Y.W. Li, M.S. Munir, "A flexible harmonic control approach through voltage-controlled DG-grid interfacing converters", IEEE Transactions on Industrial Electronics, Vol. 59, pp. 444–455, 2012.

[26] S. Rahmani, A. Hamadi, K. Al-Haddad, "A Lyapunov function-based control for a three-phase shunt hybrid active filter", IEEE Transactions on Industrial Electronics, Vol. 59, pp. 1418–1429, 2012.

[27] R.I. Leine, "The historical development of classical stability concepts: Lagrange, Poisson and Lyapunov stability", Nonlinear Dynamics, Vol. 59, pp. 173–182, 2009.

[28] C.C. Hua, C.H. Li, C.S. Lee, "Control analysis of an active power filter using Lyapunov candidate", IET Power Electronics, Vol. 2, pp. 325–334, 2009.

[29] E. Koutroulis, F. Blaabjerg, "A new technique for tracking the global maximum power point of PV arrays operating under partial-shading conditions", IEEE Journal of Photovoltaics, Vol. 2, pp. 184–190, 2012.

[30] M. Ciobotaru, R. Teodorescu, F. Blaabjerg, "A new single-phase PLL structure-based on second-order generalized integrator", IEEE Conference on Power Electronics Specialists, pp. 1–6, 2006.

[31] E. Jacobsen, R. Lyons, "The sliding DFT", IEEE Signal Processing Magazine, Vol. 20, pp. 74–80, 2003.

[32] R.H. Park, "Two-reaction theory of synchronous machines generalized method of analysis-part I", Transactions of the American Institute of Electrical Engineers, Vol. 48, pp. 716–727, 1929.

[33] IEEE, IEEE Recommended Practices and Requirements for Harmonic Control in Electrical Power Systems, IEEE Std 519-1992, 1993.